Gaussian Field Current Estimation from Drift Sea Ice Tracking with the Labeled Multi-Bernoulli Filter

Jonatan Olofsson*, Andreas Lindahl Flåten*, Clas Veibäck†, Tom Rune Lauknes‡

* Center for Autonomous Marine Operations and Systems (NTNU-AMOS)
Department of Engineering Cybernetics,
Norwegian University of Science and Technology, Trondheim, Norway.
jonatan.olofsson@ntnu.no, andreas.flaten@itk.ntnu.no

† Department of Automatic Control,
Linköping University, Linköping, Sweden.
clas.veiback@liu.se

‡ Norut, Tromsø, Norway.
tom.rune.lauknes@norut.no

***Abstract*—In polar region operations, drift sea ice positioning and tracking is useful for both scientific and safety reasons. Modeling ice movements has proven difficult, not least due to the lack of information of currents and winds of high enough resolution. Thus, observations of drift ice is essential to an up-to-date ice-tracking estimate.**

As an inverse problem, it is possible to extract current and wind estimates from the tracked objects of a Multi-Target Tracking (MTT) filter. By inserting the track estimates into a Gaussian field, we obtain a two-dimensional current estimate over a region of interest.

The algorithm is applied to a Terrestrial Radar Interferometer (TRI) dataset from Kongsfjorden, Svalbard, to show the practical application of the current estimation.

I. Introduction

Work in the polar regions of our planet is unavoidably linked with hazards such as drift ice. Increased presence fueled by economic interests in the Arctic, has for several decades called for research in the field of Ice Management [14]. A comprehensive overview of Ice Management in practical use is provided in [3]. The field deals with the detection, tracking and forecast of ice, but also the physical actions taken to avoid collisions [3].

For tracking sea ice movements, multiple sensors have been studied — such as satellite-carried Synthetic Aperture Radar (SAR) [12], Unmanned Aerial Systems (UAS's)[7, 5, 9] and, as studied in this paper, Terrestrial Radar Interferometer (TRI) [20]. The implementation is applied to a TRI dataset provided by Norut, exemplified in Figure 1. The extraction of detections from the imagery is detailed in Section II.

The detections are tracked in time using a Labeled Multi-Bernoulli LMB filter — presented in Section III. From the tracking of the ice obects, it is possible to extract position and velocity estimates. These can be used to estimate a Gaussian velocity field which can be interpreted as the result of currents and/or winds. This field can be used for user presentation, but potentially also for motion modeling and prediction — albeit with a risk of filter information looping. This system is outlined in Figure 2.

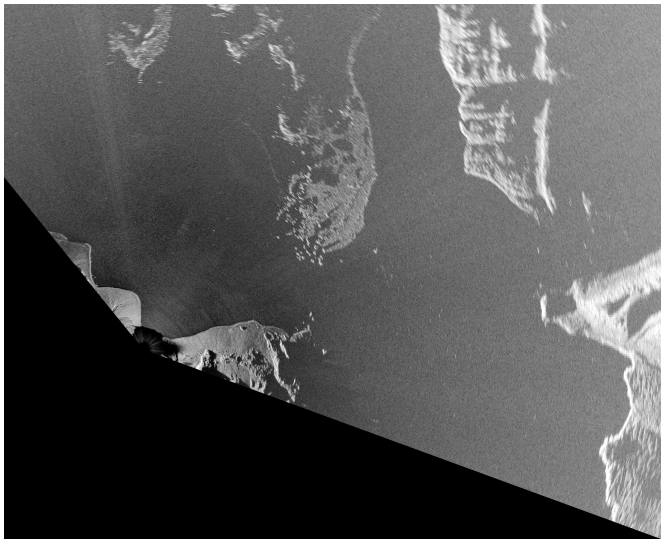

Figure 1: Example data from the Norut TRI dataset.

The theory of Gaussian fields is briefly presented in Section IV and then applied in Section V where the tuning and results are presented.

II. Sea Ice Detection

In April 2016, the partners of the Norwegian Centre for Integrated Remote Sensing and Forecasting for Arctic Operations — CIRFA — conducted a field campaign in Kongsfjorden on Svalbard. One of the datasets collected is from a GAMMA Portable Radar Interferometer (GPRI). As an application, we study the extraction of ice detections from this data and its tracking with the LMB

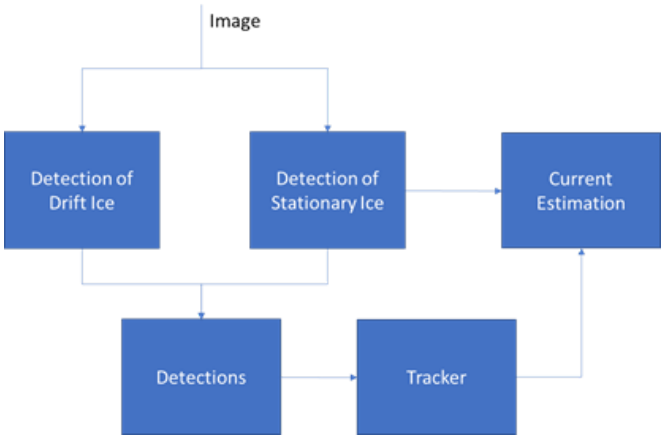

Figure 2: System outline. Scans are reported from multi-target sensing sensors and tracked in an LMB filter. This information is then extrapolated through a Gaussian field current estimation model and evaluated and displayed to the user.

filter. This dataset has been previously presented in [13], but is briefly recapitulated here for completeness.

A. Pre-processing

Each scan is delivered as the intensity of the response along range and azimuth transformed into Cartesian coordinates. From this, detections are extracted from the raw signal in a pre-processing step, through standard image processing methods.

Two types of ice are considered; 1) large regions of stationary sea ice with high signal-to-noise ratio that can be segmented independently for each scan and 2) drift ice with low signal-to-noise ratio that require pre-processing over several scans for detection. A land mask is applied to the image to ensure that detections are only obtained in water regions.

1) Detection of Stationary Sea Ice: Large areas of stationary ice are visible in the water, in particular in proximity to land. However, due to speckle noise and varying intensity over the image a simple threshold results in poor performance. To improve the signal-to-noise ratio, a sequence of standard image segmentation methods [4] are applied [13] to average, filter and extract areas considered stationary over an extended period of time.

2) Detection of Drift Ice: Drift ice is generally small and often difficult to distinguish in the speckle noise. In the dataset, a background model is estimated in water regions, modelling each pixel as a mixture of Gaussian distributions [8, 17]. A simplified expectation-maximization method [1] is then used to continuously estimate the means and covariances in the model over time. For an incoming scan, all pixels that are significantly different from their background models are segmented as foreground. This implies many false detections, which is mitigated by extracting connected components of a minimum size of $150\,\mathrm{m}^2$. The reports are then obtained as the centroid of each connected component.

III. The Labeled Multi-Bernoulli Filter

To track point-target ice-objects in the data, the LMB filter is employed, although many MTT algorithms exist that would provide a comparable level of accuracy and performance. The LMB filter was proposed in [16] as a simplification of the δ-GLMB-filter [19, 18], and the implementation used is outlined in [13].

A. Outline

The LMB filter is defined in the framework of Finite Set Statistics (FISST) [16], of which the Random Finite Set (RFS) is an integral part. An RFS is a set with a probabilistic cardinality distribution, i.e. each potential element is included in the set with a given probability. Specifically, a Bernoulli RFS is a random set which is empty with probability $1-r$, and with probability r is a singleton. For an element x with probability $p(\cdot)$, the Bernoulli RFS pdf is given by

$$\pi(X) = \begin{cases} 1-r & \text{if } X = \emptyset \\ r \cdot p(x) & \text{if } X = \{x\} \end{cases}. \tag{1}$$

A multi-Bernoulli RFS is the resulting set of the union of M independent Bernoulli-distributed random finite sets $X^{(i)}$: $X = \bigcup_{i=1}^{M} X^{(i)}$. Consequently, the multi-Bernoulli RFS is parametrized by the set $\left\{\left(r^{(i)}, p^{(i)}\right)\right\}_{i=1}^{M}$, and its pdf is given by [11]

$$\pi(\{x_1, \ldots, x_n\}) = \prod_{j=1}^{M}\left(1 - r^{(j)}\right) \times \sum_{1 \le i_1 \neq \cdots \neq i_n \le M} \prod_{j=1}^{n} \frac{r^{(i_j)} p^{(i_j)}(x_j)}{1 - r^{(i_j)}}. \tag{2}$$

The labeled multi-Bernoulli is obtained by the augmentation of each Bernoulli RFS with a unique label, $\ell \in \mathcal{L}$. The LMB RFS can thus be described by the set

$$\left\{\left(r^{(\ell)}, p^{(\ell)}\right)\right\}_{\ell \in \mathcal{L}}.$$

This set fully describes a multi-target probability density, $\pi(X)$, which can be written with the following the shorthand notation $\pi = \left\{\left(r^{(\ell)}, p^{(\ell)}\right)\right\}_{\ell \in \mathcal{L}}$, representing the current best estimate of 1) possible target state distributions, and 2) the probability of each member corresponding to a true target.

The LMB filter follows the classical predict/correct filter recursion after each of which an updated LMB RFS is obtained. The specifics of each step is presented in e.g. [13, 16].

B. Model

The drift ice is modelled as having a discrete nearly constant velocity subject to zero-mean white-noise acceleration, as discretized from the continuous-time nearly-constant-velocity model [10]. The states in the model are position and velocity in two dimensions, and the sensor is modelled to directly measure the position of the drift ice with zero-mean Gaussian noise.

The sampling time of the motion model is 180 s, matching the sample rate of the TRI sensor. The motion model covariance parameter is chosen, through manual tuning, in both dimensions as $1.7 \times 10^{-5}\,\mathrm{m}^2/\mathrm{s}^3$ and the measurement noise standard deviation is chosen as 12.2 m in each dimension.

C. Implementation

The implementation of the LMB that was used in this paper is available under a Free and Open-Source Software (FOSS) license at https://github.com/jonatanolofsson/lmb. Notably, it uses a spatially indexed storage which facilitates a scalable correction update. This spatial indexing can also be used for a scalable calculation of the Gaussian field.

IV. Gaussian Fields

The LMB filter estimates positions and velocities of detections in the scene — properties which can be input into a Gaussian field for the estimation of a continous field of forces acting upon the ice objects in the region — currents or wind.

Gaussian fields is the extension of Gaussian processes into multi-dimensional space, and the standard equations of Gaussian processes are straightforwardly applied by simply extending the state vectors and covariances accordingly.

A Bayesian method by nature, Gaussian fields can be used to estimate the value of a vector field function at given points but also an estimated measure of the uncertainty of this estimate — its covariance. In essence, for a given point of interest, a Gaussian process/field uses the function values of other points and their associated covariances to create a weighted estimate of the function value at the point of interest.

In its simplest form, each dimension of the vector field is separable into independent Gaussian processes although in general, covariance between the dimensions must be taken into account if the dimensions are not fully statistically independent.

Given points X where the vector field has been measured to be y (except for a mean, which may be removed and added back at the end) — and points of interest in X_* where we want to evalate the estimated underlying function — the formula, from which the concept of Gaussian processes and fields are derived, is the joint Gaussian:

$$\begin{bmatrix} y \\ f_* \end{bmatrix} \sim \mathcal{N}\left(0, \begin{bmatrix} K & K_* \\ K_*^T & K_{**} \end{bmatrix}\right), \tag{3}$$

where f_* is a vector of the (concatenated) vector-field values at the points of interest, and $K = \mathrm{cov}\,(y, y)$, $K_* = \mathrm{cov}\,(y, f_*)$, $K_{**} = \mathrm{cov}\,(f_*, f_*)$ [15].

This leads, for the points in X_*, to the predictive equation [15] of

$$f_* | X, y, X_* \sim \mathcal{N}\left(\bar{f}_*, \mathrm{cov}\,(f_*)\right), \text{ where} \tag{4}$$

$$\bar{f}_* \triangleq K_*^T K^{-1} y, \tag{5}$$

$$\mathrm{cov}\,(f_*) = K_{**} - K_*^T K^{-1} K_*. \tag{6}$$

I.e., $\bar{f}_*$ contains the mean of the estimated vectors at the points in X_*, and $\mathrm{cov}\,(f_*)$ contains their joint covariance. In the application of this paper, we see the velocity estimates as the measurements y, taken at the estimated position of each target track — X.

For Gaussian processes, the matrices K_* and K_{**} are predominantly generated by standard covariance functions — *kernels* —, functions of point pairs which together form valid covariance matrices [2], each element being

$$\begin{aligned} K_{i,j} &= k\,(x_i, x_j) \\ &= \mathrm{cov}\,(f\,(x_i)\,, f\,(x_j))\,, \end{aligned} \tag{7}$$

where f is the estimated underlying function

$$f\,(x) \sim \mathcal{GP}\,(m\,(x)\,, k\,(x, x')) \tag{8}$$

for a specified mean function m. In the N-dimensional case, $K_{i,j}$ instead represents the $N \times N$-dimensional submatrix with its upper left corner at $(N \cdot i, N \cdot j)$.

As an example kernel, the squared exponential (SE) kernel for points x, x' is defined in one dimension as

$$k_{\mathrm{SE}}\,(x, x') = \sigma^2 \exp\left(-\frac{(x - x')^2}{2\ell^2}\right), \tag{9}$$

parametrized by the hyperparameter l. This can be extended to the multi-dimensional case

$$\boldsymbol{k}_{\mathrm{SE}}\,(\boldsymbol{x}, \boldsymbol{x}') = P \exp\left(-\frac{1}{2}(\boldsymbol{x} - \boldsymbol{x}')^T L^{-1}\,(\boldsymbol{x} - \boldsymbol{x}')\right), \tag{10}$$

with P being the covariance matrix at $\boldsymbol{x}$ and L being the scaling and rotation of the bell-shaped attenuation when moving away from $\boldsymbol{x}$. Other kernels may be extended analogously.

Note that the points are not necessarily in space — kernels may defined in any dimension. For example, a kernel may defined for the time dimension to represent a time dependency with a forgetting factor.

While kernels, and combination of kernels [2], is the standard way of forming the submatrices of (3), the predictive equations are valid for all valid (co)variance matrices. For example — and relevantly — the uncertainty of the filtered velocity estimates of Section III may be incorporated in the K and K_* matrices. For the LMB velocity covariance, this corresponds to the case of noisy measurements in the Gaussian process [15]. Another noise source comes from the uncertainty in position. However,

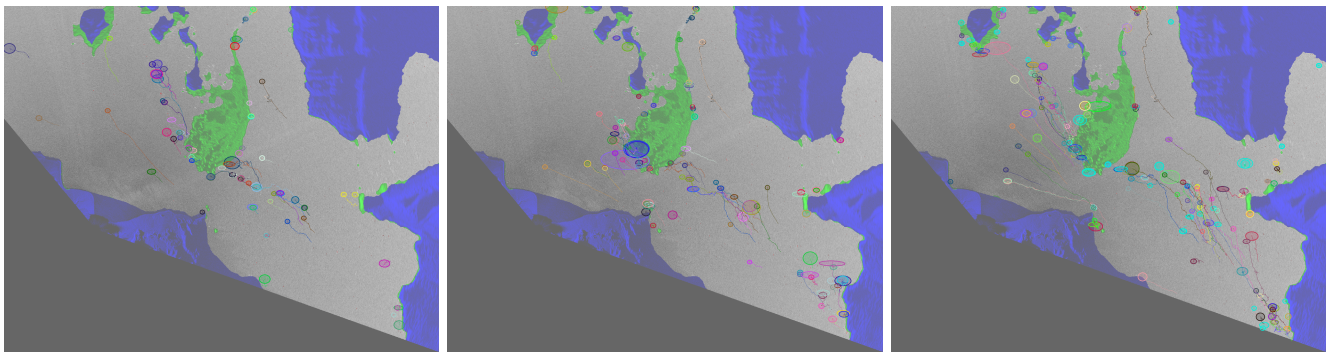

(a) Tracks after 2 h. (b) Tracks after 4 h. (c) Tracks after 7 h.

Figure 3: Drift ice tracks over time, showing the land mask in blue and stationary detections in green. Tracks and targets retain an individual randomly assigned color over time.

a detailed handling of this is less straightforward and thus currently only taken into account indirectly through the general kernel.

V. Results

This section describes the evaluation of the application of Gaussian fields to a TRI dataset collected by the Norwegian research institute Norut at Kongsfjorden, Svalbard.

From the dataset, detections are extracted and tracked with the LMB filter to generate tracks with estimated velocities and positions. The estimated target velocities are used to form a Gaussian field of velocities, observed at the target's positions.

In [13], an ice tracker was developed for the use on this dataset. The results are exhibited in Figure 3.

A variation of kernel choices and kernel parametrization is evaluated against a score for comparing the predictive qualities of the model. Given a velocity prediction and a verification vector — $\bar{v}$ and v respectively, with associated covariances $P_{\bar{v}}$ and P_v — the optimal prediction is obtained when $\bar{v} = v$. A description of the distribution difference is the innovation between the two, which in the Gaussian case is formed by the Gaussian distribution

$$\mathcal{N}\left(\bar{v} - v; 0, P_{\bar{v}} + P_v\right) = \mathcal{N}\left(\tilde{v}; 0, \Sigma\right).$$

A similarity score may be devised from the negative log likelihood of the innovation:

$$\gamma = \frac{1}{2}\left(\ln|\Sigma| + \tilde{v}^T\Sigma^{-1}\tilde{v} + 2\ln 2\pi\right) \tag{11}$$

The total score is created for each frame — repeatedly in Monte Carlo fashion — by putting aside 25 % of the detections for a verification dataset and averaging the score they receive when compared to the predictions from the Gaussian field.

For the predictive modelling of the iceberg motion, the following kernels were considered in particular (for $r = |x - x'|$, hyperparameter l):

Exponential (EXP)	$e^{-r/l}$
Squared Exponential (SE)	$e^{-(r/l)^2}$
Corrected Inverse Distance (CID)	$\left(1 + \frac{r}{l}\right)^{-1}$
Rational Quadratic (RQ)	$\left(1 + \frac{r^2}{l^2}\right)^{-1}$

Additionally, the kernels were combined with a CID kernel over the time dimension. In these cases, historical data from the LMB tracks were used for additional data.

The above kernels were tested — with and without time kernel — for a variation of physically reasonable hyperparameter settings. The results are summarized in Table I and exemplified in Figure 4 (kernels with a time factor are suffixed by *T*.).

Kernel	Score	Score cov.	Relative, %
EXP(400)	5.09175	0.0189955	101.105
EXP(750)	5.10378	0.0181352	101.344
EXP(1200)	5.12499	0.0369751	101.765
SE(200)	6.10111	23.3351	121.147
CID(100)	5.07517	0.0204076	100.775
CID(400)	5.07999	0.0274274	100.871
CID(900)	5.11524	0.0307042	101.571
RQ(200)	5.57251	0.578188	110.651
EXPT(400, 30)	5.05754	0.0236918	100.425
EXPT(750, 30)	5.07125	0.0203695	100.698
EXPT(1200, 30)	5.07709	0.0217448	100.813
CIDT(100, 30)	5.03612	0.0145595	100
CIDT(400, 30)	5.05708	0.0216197	100.416
CIDT(900, 30)	5.0955	0.0224501	101.179

Table I: Score chart for a selected sample of kernels and hyperparameters. A lower score indicates a better match, and a lower covariance indicate consistent performance. Kernel distance hyperparameters are given in meters and minutes respectively. With multiple similar scores, the comparison is inconclusive for a single best setting.

The best matches to the verification set are obtained through the use of an exponential or a CID kernel, altough for this specific dataset, similar scores are obtainable from different parameter settings. In our simulations, the rapid decline in correlation with the squared exponential kernel was so severe that it caused numerical problems with an l hyperparameter outside the tested range. Thus, only values up to 200 m were tested.

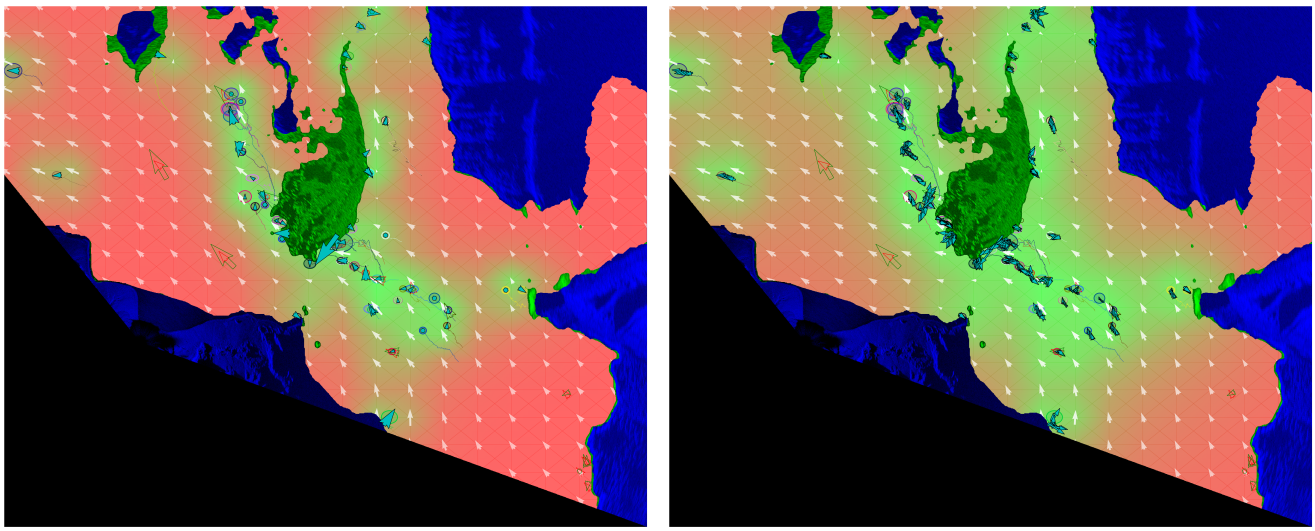

(a) EXP(750 m)

(b) CIDT(1000 m, 90 min)

Figure 4: Using two example kernels, these images exemplify the resulting velocity vector field attained from the Gaussian field. The blue area represents the masked land, the green area the stationary ice and the blue arrows the ice objects used for training the Gaussian field. The verification set and their projected estimates are green and red arrows respectively. The background — ranging from red (high) to green (low) — is determined by the trace of the Gaussian field velocity covariance in each point, thus representing the inverse of the level of information available at each point.

VI. Conclusions

This paper presents a follow-up for the [13] paper — exploring the extension of MTT state estimation into Gaussian field prediction modelling — and presents an abbreviated introduction to the application of Gaussian fields as a method of modeling ice motion over an observed region, based on the input of tracked ice objects.

Based on the available observations, the Gaussian field provides a continous representation of the predicted object velocities of an area.

Due to the lack of precise information about for example ice object size and weight, it is difficult to draw precise predictive conclusions about other, or future, ice objects as the forces will act differently depending on object size and other physical properties. One remedy for this may be to include information about e.g. Hu moments [6] and use this information in the kernels as measures of inter-object proximity. The steady-state assumption that corresponds to assuming similar speeds of nearby ice-objects appears, however, to work reasonably well in practice.

As it is its main input, the performance of the Gaussian field model is strongly dependent on the quality of the tracker. Further tuning, testing and verification of both the tracker and the Gaussian field model is still required to attain a general result which confidently describes the scenario. One potential improvement, for scalability as well as improved results, would be to create a more local model of the velocity mean. Currently the mean is shared throughout the entire dataset. Relevantly, a major limiter for using Gaussian fields with large datasets is the computational burden of inverting large matrices and this can partially be remedied through the use of gating — a process in which only the points which most affect the result are selected to create a considerably smaller matrix to invert, at the same time yielding more local results for each point. This gating can be naturally facilitated with the spatially indexed storage in the LMB implementation used in this paper.

The application of Gaussian models are often automated through the optimization of the kernel hyperparameters using e.g. Monte Carlo optimization. This is of course relevant here, although must be combined with the manual addition of the experience and understanding of relevant hyperparameter intervals. It also requires datasets of significant size, which is not yet available for this particular application.

With parameter tuning, very similar results can be obtained with different kernels. The similarities in scores also indicates that in this dataset, the velocities are generally not too far from the mean. Thus, rather than conclude a specific best kernel choice for this application, we chose to focus on the general process of combining the multi-target tracking with Gaussian fields to attain a velocity field model over the observed region.

Future work include two primary aspects: the feedback of the Gaussian field to the LMB filter for ice motion prediction, and its use for the planning of information acquisition. In the first case, the velocity model obtained in the Gaussian field can be utilized e.g. in the initialization of new targets in the tracker, providing an improved

model for initiating new targets from a single detection where velocity data is otherwise unavailable.

In the second case, we can see the Gaussian field covariance measure as an inverse metric of information. This metric can be employed in an optimization routine to plan the route of one or more moving sensor agents, to maximize the information gain.

Acknowledgments

This project has received funding from the European Union's Horizon 2020 research and innovation programme under the Marie Sklodowska-Curie grant agreement No 642153, as well as the Research Council of Norway through the Centres of Excellence funding scheme, grant number 223254 – NTNU-AMOS. The project has also been supported by funding from Vinnova Industry Excellence Center LINK-SIC, the Swedish strategic research center Security Link and the Swedish Research Council through the project Scalable Kalman Filters. Further, this work was supported by the Research Council of Norway through projects 223254 (Centre for Autonomous Marine Operations and Systems at NTNU) and 244116/O70 (Sensor Fusion and Collision Avoidance for Autonomous Marine Vehicles).

The TRI campaign was funded by the Fram Centre project *Ground-based radar measurements of sea-ice, icebergs, and growlers.*

References

[1] A. P. Dempster, N. M. Laird, and D. B. Rubin, "Maximum likelihood from incomplete data via the EM algorithm," *Journal of the Royal Statistical Society, Series B*, vol. 39, no. 1, pp. 1–38, 1977.

[2] D. Duvenaud, "Automatic Model Construction with Gaussian Processes," no. June, 2014. [Online]. Available: https://www.repository.cam.ac.uk/handle/1810/247281

[3] K. Eik, "Review of Experiences within Ice and Iceberg Management," *Journal of Navigation*, vol. 61, no. 04, p. 557, 2008.

[4] R. C. Gonzalez and R. E. Woods, *Digital Image Processing*, 3rd ed. Upper Saddle River, NJ, USA: Pearson Prentice Hall, 2008.

[5] J. Haugen, "Autonomous Aerial Ice Observation," Ph.D. dissertation, Norwegian University of Science and Technology, 2014.

[6] M.-K. Hu, "Visual pattern recognition by moment invariants," *IRE Transactions on Information Theory*, vol. 8, pp. 179–187, 1962.

[7] T. A. Johansen and T. Perez, "Unmanned Aerial Surveillance System for Hazard Collision Avoidance in Autonomous Shipping," 2015.

[8] P. Kaewtrakulpong and R. Bowden, "An improved adaptive background mixture model for real-time tracking with shadow detection," in *Proceedings of 2nd European Workshop on Advanced Video Based Surveillance Systems*, Sep. 2001.

[9] F. S. Leira, "Object Detection and Tracking With UAVs," Ph.D. dissertation, Norwegian University of Science and Technology, 2017.

[10] X. R. Li and V. P. Jilkov, "Survey of maneuvering target tracking. part i. dynamic models," *IEEE Transactions on Aerospace and Electronic Systems*, vol. 39, no. 4, pp. 1333–1364, Oct 2003.

[11] R. P. S. Mahler, *Statistical Multisource-Multitarget Information Fusion*. Norwood, MA, USA: Artech House, Inc., 2007.

[12] J. Olofsson, E. Brekke, T. I. Fossen, and T. A. Johansen, "Spatially Indexed Clustering for Scalable Tracking of Remotely Sensed Drift Ice," in *IEEE Aerospace Conference Proceedings*, Big Sky, MT, USA, 2017.

[13] J. Olofsson, C. Veibäck, and G. Hendeby, "Sea Ice Tracking with a Spatially Indexed Labeled Multi-Bernoulli Filter," in *Information Fusion (FUSION), 2017 20th International Conference on*, Xi'an, China, 2017.

[14] C. Randell, F. Ralph, D. Power, and P. Stuckey, "OTC 20264 Technological Advances to Assess , Manage and Reduce Ice Risk in Northern Developments," in *Offshore Tecdhnology Conference*, 2009.

[15] C. E. Rasmussen and C. K. I. Williams, *Gaussian Processes for Machine Learning*. MIT Press, 2006.

[16] S. Reuter, B.-T. Vo, B.-N. Vo, and K. Dietmayer, "The Labeled Multi-Bernoulli Filter," *IEEE Transactions on Signal Processing*, vol. 62, no. 12, pp. 3246–3260, 2014.

[17] C. Stauffer and W. E. L. Grimson, "Adaptive background mixture models for real-time tracking," in *Proceedings of the IEEE Computer Society Conference on Computer Vision and Pattern Recognition*, vol. 2, Ft. Collins, CO, USA, Jun. 1999, pp. 2246–2252.

[18] B.-N. Vo, B.-T. Vo, and D. Phung, "Labeled random finite sets and the bayes multi-target tracking filter," *IEEE Transactions on Signal Processing*, vol. 62, no. 24, pp. 6554–6567, 2014.

[19] B.-T. Vo and B.-N. Vo, "Labeled random finite sets and multi-object conjugate priors," *IEEE Transactions on Signal Processing*, vol. 61, no. 13, pp. 3460–3475, 2013.

[20] D. Voytenko, T. H. Dixon, M. E. Luther, C. Lembke, I. M. Howat, and S. de la Peña, "Observations of inertial currents in a lagoon in southeastern Iceland using terrestrial radar interferometry and automated iceberg tracking," *Computers and Geosciences*, vol. 82, pp. 23–30, 2015.